

Mass spectra and Regge trajectories of light mesons in the Bethe-Salpeter approach

Christian S. Fischer^a, Stanislav Kubrak^b, and Richard Williams^c

Institut für Theoretische Physik, Justus-Liebig-Universität Giessen, 35392 Giessen, Germany.

Received: date / Revised version: date

Abstract. We extend the calculation of relativistic bound-states of a fermion anti-fermion pair in the Bethe-Salpeter formalism to the case of total angular momentum $J = 3$. Together with results for $J \leq 2$ this allows for the investigation of Regge trajectories in this approach. We exemplify such a study for ground and excited states of light unflavored mesons as well as strange mesons within the rainbow-ladder approximation. For the ρ - and ϕ -meson we find a linear Regge trajectory within numerical accuracy. Discrepancies with experiment in other channels highlight the need to go beyond rainbow-ladder and to consider effects such as state mixing and more sophisticated quark-antiquark interaction kernels.

PACS. 12.38.Lg – 14.40.Be – 14.40.Df

1 Introduction

Understanding the formation and the structure of hadronic bound-states is one of the most interesting – and difficult – tasks within QCD. In any gauge-fixed approach to QCD it involves the charting of the underlying non-perturbative interactions between quarks and gluon and requires an understanding of the associated phenomena of dynamical quark mass generation and confinement. The simplest color neutral state of QCD is the meson, consisting of a quark and an antiquark, which gives rise to particular combinations of quantum numbers J^{PC} often characterized within the quark model. However, similar (and exotic) quantum numbers may arise for so-called hybrid states that contain one or more constituent gluons, as well as more complex ones such as glueballs, meson molecules and tetraquarks. These states may mix into each other, thus providing a rich and complicated spectrum explored in many experiments.

This may be particularly true for the light meson sector, where a huge amount of literature is available dealing with this problem. Relativistic quark models, effective chiral Lagrangians, Hamiltonian approaches, QCD sum rules, Dyson-Schwinger and functional renormalisation group methods as well as lattice QCD are methods of choice, see *e.g.* [1] for a recent review and a guide to further reading. In this work we concentrate on the functional approach via Dyson-Schwinger equations (DSEs) and Bethe-Salpeter equations (BSEs), which offers the above-mentioned direct connection between the details of

the non-perturbative quark-gluon interaction and the relativistic and field-theoretical description of bound-states.

The purpose of this work is twofold. On the one hand, we report on an important technical extension: to the well-known representations of (pseudo-)scalar, (axial-)vector and (pseudo-)tensor states [2–5] we add an explicit basis construction for mesons with $J = 3$. This allows, for the first time, the explicit study of Regge-trajectories in the DSE/BSE framework. For the light meson sector this may be especially interesting, since the conventional picture of a linear rising potential associated with a flux tube that underlies intuitive explanations of linear Regge-type behavior hardly seems appropriate. This is, however, the mechanism that is built into relativistic quark models relying on linear rising (quasi-)potentials, see *e.g.* [6, 7]. In contrast, an approach like the DSE/BSE framework offers the opportunity to explore alternative mechanisms for the generation of Regge-type behavior from the underlying quark-gluon interaction.

On the other hand, we explore the spectrum of ground and excited states of light mesons with total angular momentum $J = 0, 1, 2, 3$ starting from the simplest of all truncations, namely a rainbow-ladder framework with a flavor-diagonal interaction. It has the merit of preserving chiral symmetry in the form of the axial-vector Ward-Takahashi identity thus reproducing important QCD constraints such as the (pseudo-)Goldstone boson nature of the pseudoscalar mesons and the associated Gell-Mann–Oakes–Renner relation. However, it has been noted previously (see *e.g.* Refs. [8, 9] and Refs. therein) that apart from the ground state pseudoscalar and vector channels, this truncation may have serious shortcomings that prevent close quantitative contact with experiment. In this

^a e-mail: christian.fischer@theo.physik.uni-giessen.de

^b e-mail: stanislav.kubrak@theo.physik.uni-giessen.de

^c e-mail: richard.williams@theo.physik.uni-giessen.de

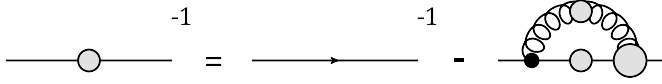


Fig. 1. The Dyson-Schwinger equation for the fully dressed quark propagator. Wiggly lines represent gluons and straight lines quarks. Large filled circles indicate the quantity is fully-dressed, otherwise it is bare.

work we explore this issue for a wide range of different channels and confirm previous work. However, including the $J = 3$ results we are able to identify a larger pattern that leads to different conclusions than those made in [8] regarding the precise origin of the shortcoming of the rainbow-ladder truncation. This is detailed below.

The paper is organized as follows. In section 2 we introduce the framework of the DSEs and BSEs, together with a discussion of the Rainbow-Ladder truncation and the model interaction employed. In section 3 we present the covariant decomposition of the Bethe-Salpeter amplitude for $J = 0, 1, 2$, as well as $J = 3$. Our numerical methods are discussed in section 4 with results given in section 5. We conclude in section 6.

2 Framework

We work in Euclidean space with the dressed one-particle irreducible Green's functions of QCD. These are obtained through solutions of their corresponding DSEs, employing truncations that are designed to maintain important symmetries of QCD such as chiral symmetry. The resulting Green's functions serve as input into the BSE for bound states of a quark and an anti-quark. In the following we summarize the corresponding formalism and give details on the approximation scheme used.

2.1 Quark propagator

The dressed quark propagator is given by

$$S^{-1}(p) = Z_f^{-1}(p^2) (i\not{p} + M(p^2)) , \quad (1)$$

where the quark wave function is $Z_f(p^2)$ and its mass function $M(p^2)$. The bare quark propagator is obtained by setting $Z_f(p^2) = 1$ and $M(p^2) = m_0$, with the bare quark mass m_0 related to the renormalized quark mass m_q via $Z_2 m_0 = Z_2 Z_m m_q$ via the renormalization factors Z_2 and Z_m . The dressing functions $Z_f(p^2)$ and $M(p^2)$ are obtained as a solution of the quark DSE

$$S^{-1}(p) = Z_2 S_0^{-1} + g^2 Z_{1f} C_F \int_k \gamma^\mu S(k) \Gamma^\nu(k, p) D_{\mu\nu}(q) , \quad (2)$$

given pictorially in Fig. 1. Here we use the abbreviation $\int_k = \int d^4k / (2\pi)^4$ and the momentum routing $q = k - p$. The gluons propagator is denoted by $D_{\mu\nu}(q)$ and $\Gamma^\nu(k, p)$

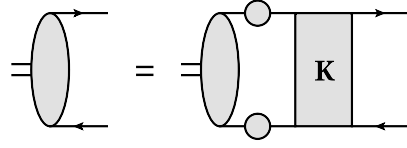


Fig. 2. The homogeneous Bethe-Salpeter equation for a bound-state of a quark and an antiquark. The quark-antiquark interaction kernel K is constrained by requirements of chiral symmetry.

the dressed quark-gluon vertex. The corresponding renormalization factor is Z_{1f} . The Casimir factor $C_F = 4/3$ stems from the color trace and g is the renormalized coupling of QCD.

We work in Landau gauge, where the gluon propagator is purely transverse and given by

$$D_{\mu\nu}(q) = \left(\delta_{\mu\nu} - \frac{q_\mu q_\nu}{q^2} \right) \frac{Z(q^2)}{q^2} = T_{\mu\nu}^q \frac{Z(q^2)}{q^2} , \quad (3)$$

with transverse projector $T_{\mu\nu}^q$.

2.2 Bethe-Salpeter equation

The Bethe-Salpeter equation, given in Fig. 2, describes a relativistic bound-state of mass M calculated through

$$[\Gamma(p; P)]_{tu} = \lambda \int_k K_{rs;tu}^{(2)}(p, k; P) [\chi(k; P)]_{sr} . \quad (4)$$

Here, $\Gamma(p; P)$ is the Bethe-Salpeter amplitude, $\chi(k; P) = S(k_+) \Gamma(k; P) S(k_-)$ the corresponding wave function and $K^{(2)}$ a two-particle irreducible quark anti-quark interaction kernel. The momenta $k_\pm = k + (\xi - 1/2 \pm 1/2)P$ feature a momentum partitioning parameter ξ , which has no influence on the bound state mass. The BSE is a homogeneous eigenvalue equation with a discrete spectrum of solutions at momenta $P^2 = -M_i^2$ and eigenvalues $\lambda(P_i^2) = 1$. The lightest of these M_i is the ground state solution. For a bound state with total angular momentum J , both $\Gamma(p; P)$ and $\chi(k; P)$ have J Lorentz indices. Their covariant decomposition is a combination of the Dirac representation for two composite spin-1/2 fermions and an angular momentum tensor.

2.3 Rainbow-Ladder

The essential input into the DSE for the quark propagator and the interaction kernel of the two-body Bethe-Salpeter equation is the dressed gluon propagator and the dressed quark-gluon vertex. Both the quark self energy and the interaction kernel $K^{(2)}$ are related by the axial Ward-Takahashi identity (axWTI). Any meaningful approximation of these quantities in the light quark sector has to satisfy this identity, otherwise essential QCD properties of dynamical chiral symmetry-breaking such as the

(pseudo-)Goldstone nature of the pion and the Gell-Mann-Oakes-Renner relation are lost. The simplest construction principle to satisfy the axWTI is the rainbow-ladder approximation, which is tantamount to taking into account only the γ_μ -structure of the dressed quark-vertex and combining all dressing effects of the gluon and the vertex into an effective running coupling. The rainbow-ladder approximation is simple to use and we will therefore employ it in this exploratory study. Its merits and deficiencies have been indicated already in the introduction and will be discussed in more detail in the results section.

For completeness let us mention, that there have been many efforts to go beyond rainbow-ladder. One promising route is to use explicit diagrammatic approximations to the DSE of the quark-gluon vertex [10–17]. This allows the explicit study of the effects of the gluon self-interaction [16] as well as pion cloud effects [17] on the spectrum of light mesons and baryons [18]. Another promising approach uses explicit representations of selected tensor structures of the quark-gluon vertex beyond the leading γ_μ piece [19–22]. As will be clear from the results section it is mandatory to repeat the meson survey performed here in one or more of the above approaches in future work.

In rainbow-ladder approximation the relevant parts in the quark self-energy simplify according to

$$Z_1 f C_F \frac{g^2}{4\pi} D_{\mu\nu}(q) \Gamma^\nu(k, p) = Z_2^2 C_F T_{\mu\nu}^q \frac{\alpha_{\text{eff}}(q^2)}{q^2} \gamma^\nu, \quad (5)$$

where we also collected together some numerical constants and the color traces. The corresponding two-body kernel, consistent with chiral symmetry, is given by

$$K_{rs;tu}^{(2)}(p, k; P) = 4\pi Z_2^2 C_F \frac{\alpha_{\text{eff}}(q^2)}{q^2} T_{\mu\nu}^q [\gamma^\mu]_{rt} [\gamma^\nu]_{su}, \quad (6)$$

and is a function of $q = k - p$ only. In particular, we take the model interaction of Maris and Tandy [23]

$$\alpha_{\text{eff}}(q^2) = \pi\eta^7 x^2 e^{-\eta^2 x} + \frac{2\pi\gamma_m (1 - e^{-y})}{\log[e^2 - 1 + (1 + z)^2]}, \quad (7)$$

where $x = q^2/\Lambda^2$, $y = q^2/\Lambda_t^2$, $z = q^2/\Lambda_{\text{QCD}}^2$. Here $\Lambda_t = 1$ GeV is a regularization parameter for the perturbative logarithm; its value has no material impact on the numerical results. The QCD-scale $\Lambda_{\text{QCD}} = 0.234$ GeV controls the running of the logarithm with anomalous dimension $\gamma_m = 12/25$ corresponding to four active quark flavors. The infrared strength of this model is controlled by the parameters Λ and η . While $\Lambda = 0.72$ GeV is fixed from the pion decay constant, there is considerable freedom to vary the dimensionless parameter η . We will use $\eta = 1.8 \pm 0.2$ for which ground-state observables are insensitive and discuss the effects of this variation on the excited states.

3 Covariant Bethe-Salpeter amplitude

It is well known that composite states of particles in the $(j, 0) \oplus (0, j)$ -representation can be constructed by forming direct products of the particle's representation [2, 3].

For fermions, $j = 1/2$, this reduces to the Dirac spinor formalism and thus is given by the usual Dirac matrices.

For a meson in the rest frame with center-of-mass momentum t_μ and relative quark momentum r_μ , grouped by their transformation under parity we have

$$D^{(1)} = \begin{pmatrix} \mathbf{1} & t_\mu \gamma^\mu & r_\mu \gamma^\mu & r_\mu t_\nu \frac{1}{2} [\gamma^\mu, \gamma^\nu] \end{pmatrix}, \quad (8)$$

$$D^{(5)} = \begin{pmatrix} \gamma_5 & \gamma_5 t_\mu \gamma^\mu & \gamma_5 r_\mu \gamma^\mu & \gamma_5 r_\mu t_\nu \frac{1}{2} [\gamma^\mu, \gamma^\nu] \end{pmatrix}, \quad (9)$$

for scalar, $D^{(1)}$, and pseudoscalar, $D^{(5)}$, invariants respectively. Thus, for a bound-state of two fermions with definite parity, the basic number of scalar invariants equals four. Furthermore, it is convenient to replace the relative momentum r_μ by

$$Q_\mu = \tau_{\mu\nu}^{(t)} r^\nu, \quad (10)$$

where $\tau_{\mu\nu}^{(t)} = \delta_{\mu\nu} - t_\mu t_\nu / t^2$ is a transverse projector. Then, appropriate scalar and pseudoscalar invariants are

$$\bar{D}^{(1)} = \begin{pmatrix} \mathbf{1} & \not{t} & \not{Q} & \not{Q} \not{t} \end{pmatrix}, \quad \bar{D}^{(5)} = \gamma_5 \bar{D}^{(1)}, \quad (11)$$

which simplifies the operation of charge conjugation due to the property that $Q \cdot t = 0$.

Then, a bound state with zero total angular momentum and definite parity P is decomposed in terms of four components

$$\Gamma^{(P)}(r, t) = \sum_{i=1}^4 \left[\lambda_i \bar{D}_i^{(P)} \right]. \quad (12)$$

For non-zero total angular momentum J , the scalar invariants must be coupled with an angular momentum tensor. This rank J tensor, T_{a_1, \dots, a_J} , has $2J + 1$ independent components in three spatial dimensions, corresponding to the possible spin polarisations [4]. This tensor must be symmetric in all indices and traceless with respect to contraction of any pair of indices. This generalizes to $3 + 1$ dimensions by imposing transversality of each index with respect to the total momentum.

Thus, to obtain a tensor corresponding to total angular momentum J , we construct the symmetric J -fold tensor product of a transversal projector transforming like a vector, and subtract traces with respect to every pair of indices. The case $J = 1$ will provide tensors that form the building blocks for states of higher total angular momentum.

Then, in general a meson of spin $J > 0$ and parity P has eight components and is written

$$\Gamma_{\mu_1 \dots \mu_J}^{(P)}(r, t) = \sum_{i=1}^4 \left[\lambda_i Q_{\mu_1 \dots \mu_J} \bar{D}_i^{(P)} + \lambda_{i+4} T_{\mu_1 \dots \mu_J} \bar{D}_i^{(P)} \right], \quad (13)$$

where the $Q_{\mu_1 \dots \mu_J}$, $T_{\mu_1 \dots \mu_J}$ are defined below and $\lambda_i = \lambda_i(r, t)$.

3.1 Total angular momentum $J = 1$

For the case of $J = 1$ we can immediately write down the two rank 1 tensors for a bound state of two fermions: they are the transversely projected quantities Q_μ and T_μ defined

$$Q_\mu = \tau_{\mu\nu}^{(t)} r^\nu, \quad T_\mu = \tau_{\mu\alpha}^{(t)} \tau_{\alpha\nu}^{(Q)} \gamma^\nu. \quad (14)$$

Here Q is the same quantity as defined in Eq. (10) and we introduced the additional transverse projector $\tau_{\alpha\nu}^{(Q)}$ so that the resulting basis is conveniently orthogonal. The explicit components of this basis can be found *e.g.* in Ref. [23].

3.2 Total angular momentum $J = 2$

For total angular momentum $J = 2$ we construct the 2-fold tensor products of Q_{μ_i} and T_{μ_i} . Since the product of two or more T_{μ_i} is degenerate, this gives

$$\tilde{Q}_{\mu_1\mu_2} = Q_{\mu_1} Q_{\mu_2}, \quad (15)$$

$$\tilde{T}_{\mu_1\mu_2} = T_{(\mu_1} Q_{\mu_2)}, \quad (16)$$

where (\dots) denotes the symmetrization of the indices without normalization $1/J!$. To satisfy the criteria of being angular momentum tensors we then subtract the trace-part to give [5, 24]

$$Q_{\mu_1\mu_2} = \tilde{Q}_{\mu_1\mu_2} - \frac{1}{3} Q^2 \tau_{\mu_1\mu_2}, \quad (17)$$

$$T_{\mu_1\mu_2} = \tilde{T}_{(\mu_1\mu_2)} - \frac{1}{3} Q^2 \tau_{\mu_1\mu_2}. \quad (18)$$

The explicit components of this basis can be found *e.g.* in Ref. [5].

3.3 Total angular momentum $J = 3$

For total angular momentum $J = 3$ we construct the 3-fold tensor products of Q_{μ_i} and T_{μ_i}

$$\tilde{Q}_{\mu_1\mu_2\mu_3} = Q_{\mu_1} Q_{\mu_2} Q_{\mu_3}, \quad (19)$$

$$\tilde{T}_{\mu_1\mu_2\mu_3} = T_{(\mu_1} Q_{\mu_2} Q_{\mu_3)}. \quad (20)$$

To satisfy the requirements of angular momentum tensors we subtract the trace part, yielding

$$\begin{aligned} Q_{\mu_1\mu_2\mu_3} &= \tilde{Q}_{\mu_1\mu_2\mu_3} - \frac{1}{5} \tau_{(\mu_1\mu_2} \tilde{Q}_{\mu_3)}^{\kappa\kappa}, \\ &= Q_{\mu_1} Q_{\mu_2} Q_{\mu_3} - \frac{1}{5} Q^2 \tau_{(\mu_1\mu_2} Q_{\mu_3)}, \end{aligned} \quad (21)$$

$$\begin{aligned} T_{\mu_1\mu_2\mu_3} &= \tilde{T}_{\mu_1\mu_2\mu_3} - \frac{1}{5} \tau_{(\mu_1\mu_2} \tilde{T}_{\mu_3)}^{\kappa\kappa} \\ &= T_{(\mu_1} Q_{\mu_2} Q_{\mu_3)} - \frac{1}{5} Q^2 \tau_{(\mu_1\mu_2} T_{\mu_3)}, \end{aligned} \quad (22)$$

which has not been explored in this approach before. The explicit representation of this basis is given by

$$\begin{aligned} \Gamma_{\mu_1\mu_2\mu_3}^{(1)}(r, t) &= Q_{\mu_1\mu_2\mu_3} [\lambda_1 \mathbf{1} + \lambda_2 \not{r} + \lambda_3 \not{Q} + \lambda_4 \not{Q} \not{r}] \\ &+ T_{\mu_1\mu_2\mu_3} [\lambda_5 \mathbf{1} + \lambda_6 \not{r} + \lambda_7 \not{Q} + \lambda_8 \not{Q} \not{r}], \end{aligned} \quad (23)$$

with $\lambda_i = \lambda_i(r, t)$ scalar coefficients. Multiplying through by γ_5 would yield the $\Gamma_{\mu_1\mu_2\mu_3}^{(5)}(r, t)$ basis decomposition.

4 Numerical Methods

Here we give a brief summary of the numerical methods used for this work. Primarily, this concerns the solution of non-linear integral equations at complex Euclidean momenta, followed by finding eigenvalues and the corresponding eigenvectors of a linear system in matrix form. We also discuss the means by which the higher mass states are obtained.

4.1 Quark propagator for complex momenta

In the BSE due to the external total momentum of the bound state one needs to evaluate the internal propagators on the right hand side in a parabola region sketched in Fig. 3. The quark propagator at these complex momenta p^2 could be evaluated directly from its DSE, Eq. (2), provided one knows the quark propagator for spacelike Euclidean momenta $p^2 > 0$ and the quark-gluon vertex as well as the gluon propagator for complex (gluon) momenta. In general, however, this is not the case and one has to rely upon numerical input for the gluon propagator or the vertex. In order to make our procedure sufficiently general for later studies, we use an alternative strategy. We change the momentum routing in the DSE such that the external complex-valued momentum flows through the internal quark propagator. This complex shift in the quark momentum entails that a parabolic region of the complex plane is probed by the internal quark, similar to that in the BSE, see Fig. 3. The DSE is then solved iteratively either on a momentum grid inside the parabolic region [25]

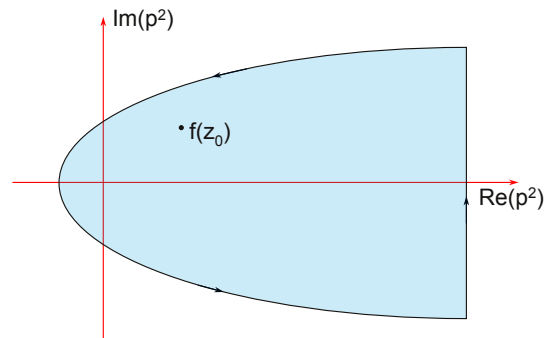


Fig. 3. Sketch of the integration contour for the determination of the quark propagator in the complex plane.

or on the boundary supplemented with Cauchy's theorem. Here, we use the latter method: given a function $f(z)$ defined on the boundary of a closed contour $z \in \mathcal{C}$, we have for any z_0 inside

$$f(z_0) = \frac{1}{2\pi i} \oint_{\mathcal{C}} \frac{dz f(z)}{z - z_0} \simeq \frac{1}{2\pi i} \sum_i \frac{w_i f(z_i)}{z_i - z_0}, \quad (24)$$

where the integral has been approximated by some quadrature formula with weights w_j and abscissa z_j . This is paired with a parametric mapping that describes the contour's boundary. Numerically this procedure poses a challenge when z_0 approaches the abscissa z_i . This can be mitigated through the use of the barycentric formula [26]

$$f(z_0) = \frac{\sum_i \bar{w}_i f(z_i)}{\sum_i \bar{w}_i}, \quad \bar{w}_i = w_i / (z_i - z_0). \quad (25)$$

If the contour \mathcal{C} is such that it encounters complex conjugate poles in the quark propagator, Eqs. (24)–(25) can be modified to include the residues. However, it is still a technical challenge to determine and include such poles numerically in a non-linear integral equation such as the quark DSE.

4.2 Calculating bound state masses

The Bethe-Salpeter equation is reduced to an eigenvalue problem for $\Gamma = \lambda M \cdot \Gamma$. The amplitude $\Gamma = \Gamma(p; P)$, for total momentum P , is a function of the relative quark momentum p and the angle $\widehat{p \cdot P}$. This angular dependence is expanded as a sum of Chebyshev polynomials, reducing the system to a coupled system of linear equations in one variable, p^2 .

The matrix M represents the coupling of this amplitude to the interaction kernel K and its subsequent integration. It is solved as an eigenvalue equation using the *Eigen* library [27]. We specify the J^P of the state through the choice of the covariant decomposition, section 3, and determine the C -parity of the state by examining the symmetry properties of the eigenvector. Excited states are obtained by finding solutions $\lambda = 1$ higher in the mass spectrum.

Since excited states, and those with $J > 2$, are typically heavy we find ourselves in the position that the parabolic region in the complex plane for which the quark propagator has been calculated is too small. The region cannot, at present, be extended due to the presence of propagator poles that must be taken into account self-consistently. A similar problem is encountered when one attempts to calculate the mass spectrum of heavy-light mesons; this is a general problem for Euclidean bound-state calculations in general within the Bethe-Salpeter framework, see [28, 29] for recent attempts to circumvent this problem.

Here, we pursue two approximations to gather information beyond this constraint. The first is to employ the Cauchy theorem for z_0 outside of the contour. Of course,

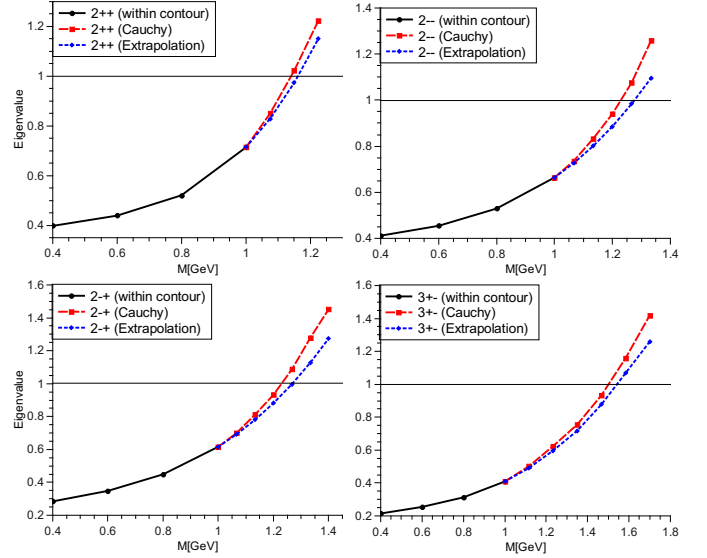


Fig. 4. Comparison of the eigenvalue curves obtained by employing the Cauchy integral formula for outside of the contour and the barycentric rational interpolation. The black curve represents the eigenvalues at masses obtained within contour.

this is only an approximate analytic continuation which, however, while not mathematically precise nevertheless culminates in well-behaved quark dressing functions.

Alternatively one can extrapolate the eigenvalue according to [9], where it was shown that linear extrapolation in $\lambda_i^{-1}(P^2) - 1$ is reliable for the pseudoscalar excited states; however this does not hold for the other channels. Therefore we used barycentric rational interpolation

$$R(x) = \frac{\sum_{i=0}^{N-1} \frac{w_i}{x - x_i} y_i}{\sum_{i=0}^{N-1} \frac{w_i}{x - x_i}}, \quad (26)$$

where w_i are the weights at desired order d are given by

$$w_k = \sum_{i=k-d}^k (-1)^k \prod_{j=i, j \neq k}^{i+d} \frac{1}{x_k - x_j}. \quad (27)$$

The comparison of these two techniques is shown in Fig. 4. As can be seen, the masses of the bound states deviate within 5–10% of the mean value with an overall tendency that the Cauchy integral formula gives a lower bound. For the purpose of the exploratory study reported here, we regard this accuracy as sufficient.

5 Results

The quantum numbers of a meson in the non-relativistic quark model are obtained from the spin, S , and relative orbital angular momentum L of the $q\bar{q}$ system, which combine to give the total spin $J = L \oplus S$. The total parity, P ,

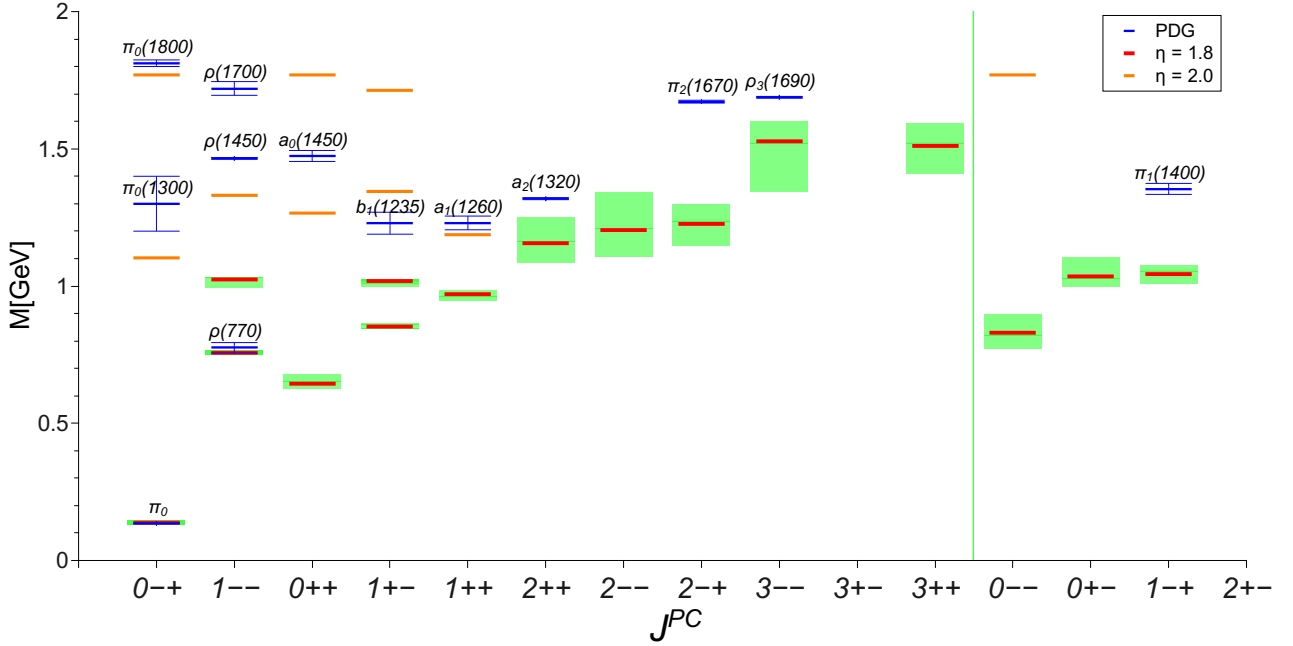


Fig. 5. (color online) (top) The calculated $n\bar{n}$ spectrum, compared to the isovector mesons as measured in experiment. The green bands correspond to the variation $\eta = 1.8 \pm 0.2$. Due to the structure of the propagator, in the case of $\eta = 2.0$ more states are accessible; these are given by the single orange lines. The states to the right of the dividing line correspond to exotic quantum numbers.

charge parity, C , and G parity are given by

$$P(q\bar{q}) = -(-1)^L, \quad (28)$$

$$C(q\bar{q}) = (-1)^{L+S}, \quad (29)$$

$$G(q\bar{q}) = (-1)^{L+S+I}, \quad (30)$$

where C parity only applies to charge neutral states and is generalized to G parity for isospin $I = 1$. Thus, the quark model yields the possible J^{PC} quantum numbers in Table 1. This leaves us with five states (for $J \leq 3$) that are considered exotic: $J^{PC} = 0^{--}$, $J^{PC} = 0^{+-}$, $J^{PC} = 1^{-+}$, $J^{PC} = 2^{+-}$, and $J^{PC} = 3^{-+}$.

5.1 Light unflavored mesons

In the RL approximation the interaction kernel admits no mixing between states. Furthermore we work in the

isospin symmetric limit using equal current quark masses $m_u = m_d = 0.0037$ GeV at a renormalization scale of $\mu = 19$ GeV. Thus, our calculated meson spectrum is degenerate in the isoscalar/isovector channel for $n = u, d$ quarks. The explicit numbers can be found in the Appendix in Table 2. In Fig. 5 we display the resulting spectrum for $n\bar{n}$ mesons, and compare with the isovector channel from experiment. The input up/down quark masses are fixed such that the experimental mass of the π_0 is reproduced. The resulting ground state mass in the vector channel is also in good agreement with experiment. This is not true, however, for the scalar and axialvector states as noted frequently before, see e.g. [11]. Here, the deficiency of the rainbow-ladder truncation is obvious and on the 20-40 % level. In the scalar channel there is some evidence that the lowest lying nonet may not be identified as simple quark-antiquark states, but may be better described as tetraquarks, see e.g. [30–34] and Refs. therein. Therefore we compare with the $a_0(1450)$, noting that in rainbow-ladder and without potential mixing with the scalar glueball state there is no hope to reproduce the experimental value. The situation is considerably better for the lowest lying tensor state [5], which for the upper value of the considered η -band is even on the 5 % level compared to the experimental value. While the other tensor states are again far off, at least where comparison with experiment is possible, the situation is again acceptable for the tensor meson with $J = 3$ and $PC = \{--\}$. Its mass of 1528^{+71}_{-184} MeV compares well with both the isovector ρ_3 of mass 1688.8 ± 2.1 MeV (shown in the figure) and the

Table 1. Allowed quantum numbers for a neutral $q\bar{q}$ state in the quark model.

L	S	J^{PC}	L	S	J^{PC}	L	S	J^{PC}	L	S	J^{PC}	L	S	J^{PC}
0	0	0^{-+}	1	0	1^{+-}	2	0	2^{-+}	3	0	3^{+-}	4	0	4^{-+}
0	1	1^{--}	1	1	0^{++}	2	1	1^{--}	3	1	2^{++}	4	1	3^{--}
			1	1	1^{++}	2	1	2^{--}	3	1	3^{++}	4	1	4^{--}
			1	1	2^{++}	2	1	3^{--}	3	1	4^{++}	4	1	5^{--}

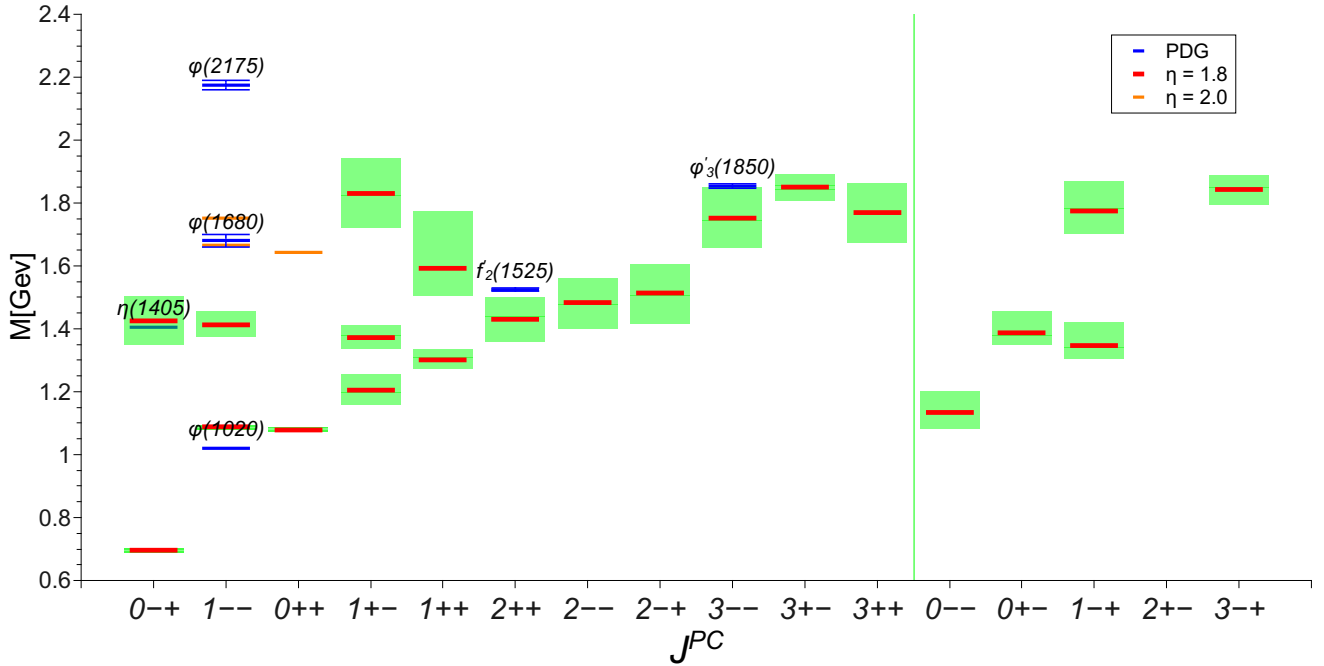


Fig. 6. (color online) Calculated $s\bar{s}$ spectrum, compared to experiment. The green bands correspond to the variation $\eta = 1.8 \pm 0.2$. Due to the structure of the propagator, in the case of $\eta = 2.0$ more states are accessible; these are given by the single orange lines. The states to the right of the dividing line correspond to exotic quantum numbers.

isoscalar ω_3 of mass 1667 ± 4 MeV with again a deviation on the 5 % level for the upper range of the η -band. In contrast, we find no bound state in the $J^{PC} = 3^{+-}$ -channel, whereas for the $J^{PC} = 3^{++}$ state with mass 1510^{+81}_{-100} MeV there is no well established experimental counterpart.

It is interesting to muse about the difference between the corresponding channels $J^{PC} = 0^{-+}, 1^{-+}$ as well as $J^{PC} = 1^{-+}, 2^{++}, 3^{-+}$ in good agreement with experiment and the other channels that are further off, using notions of the (pseudo)-potentials in the quark model. In this language, what distinguishes these channels from the others is that the non-contact part of the spin-spin interaction is vanishing or small: for the hyperfine splitting between the pseudoscalar and vector channels the contact part of the spin-spin interaction is dominant, whereas for the $J^{PC} = 2^{++}, 3^{-+}$ states the spin-orbit forces prevail. For all other channels considered, there are sizable contributions from the tensor part of the spin-spin interaction. Since these are the channels that are off, we conclude, that the rainbow-ladder interaction roughly reproduces the size of the contact part of the spin-spin interaction and the spin-orbit force, but materially overestimates the binding in the tensor part of the spin-spin interaction. Note, that this conclusion is different than the one drawn in [8] based on only a subset of the states considered here. We come back to this discussion in section 5.3.

As for the exotic channels we find states for $J^{PC} = 0^{-+}, 0^{+-}$ with no experimentally established counterpart, whereas our value for the $J^{PC} = 1^{-+}$ is about 25 % lower

than the $\pi_1(1400)$. This finding is consistent with the ones in the axial-vector channels. In the exotic channels with $J = 2, 3$ we do not find bound state.

Finally let us comment on the excited states. These are in general much too low [35] in agreement with the general finding for the ground states. A variation of the η -value in general does not improve this picture; also it is noteworthy that higher excited states only appear for very specific values of η . This suggests a dependency of the excited states on the details of the momentum and tensor dependence of the quark-gluon interaction that needs to be explored in future work.

Next we discuss the $s\bar{s}$ spectrum given in the Appendix and displayed in Fig. 6. Here the input value of the strange quark mass of $m_s(19 \text{ GeV}) = 0.085$ GeV at the renormalization point is determined from matching to the experimental value of the kaon discussed below. First note that the pseudoscalar $s\bar{s}$ -state is too light in this truncation since neither the effect of the $U_A(1)$ anomaly (see *e.g.* [36] for a treatment of the anomaly in the BSE formalism) nor flavor mixing with the $n\bar{n}$ states is considered. For the excited state in the pseudo-scalar channel the surprisingly excellent agreement with the $\eta(1405)$ extracted from experiment may be accidental. In the vector channel, where mixing effects do not play a major role we observe good agreement of our bound state mass with experiment. The same is true for the $J^{PC} = 2^{++}$ and $J^{PC} = 3^{-+}$ channels, where the upper boundary of the η -band almost reproduces the experimental values for the $f_2(1525)$ and the $\phi_3(1850)$. Again, these are the channels with dominating

spin-orbit forces in the language of the potential models. In general, the pattern of states in the $s\bar{s}$ spectrum is very similar to the one found for the $n\bar{n}$ mesons due to the flavor independence of the underlying rainbow-ladder interaction model.

5.2 Strange Mesons

In the case of strange mesons, $n\bar{s}$, one is no longer able to assign either C or G parity to a state. Thus, here there are no states with explicitly exotic quantum numbers.

The spectrum, as calculated within the rainbow-ladder approximation, is given in Fig. 7. As already mentioned above, the strange quark mass is chosen such that the calculated $K^{0,\pm}$ is in agreement in experiment; the remaining spectrum is a result of the model. While the vector ground state is in reasonable agreement with experiment, the remaining spectrum does not fare so well (as in the unflavored case).

Along with the usual $J = 1$ and $J = 2$ mesons, we find two states with $J = 3$, one with positive and one with negative parity. For the latter, we have a mass of 1646.9 (found for $\eta = 2.0$ only) which compares well with the experimentally known K_3^* whose mass 1776 ± 7 is within 10%. The positive parity state is similar in mass, 1673.4, but the putative K_3 has not been seen in experiment.

The results strongly indicate that the $n\bar{s}$ system should be investigated in a beyond rainbow-ladder approximation, in order to find stronger agreement for the majority of low-lying states. In particular, the 2^+ channel is interesting since the experimentally observed states are considerably higher in mass than the calculated ones, in contrast to the findings discussed before in the flavor diagonal channels. On the other hand, our numerical error in extracting the bound state masses is considerably higher in the non-diagonal flavor case than in the diagonal one such that it is not clear whether the deficiency is in the interaction or in our numerical procedure. This needs to be explored further.

5.3 Regge trajectories

Finally, we present results for Regge trajectories in Fig. 8 for natural parity states. We only take into account trajectories with at least three states, which leaves the ground state isovector $n\bar{n}$ and isoscalar $s\bar{s}$ mesons with natural parity; for the corresponding excited states and the other channels we do not have enough bound states with $J = 2, 3$ to probe for trajectories. One immediately notes that, indeed, the sequence $J^{PC} = 1^{--}, 2^{++}, 3^{--}$ forms an almost linear trajectory in the (M^2, J) -plane. This is interesting, since we are working with a model that is apparently *not* related to a linear rising potential between light quarks. Thus, the conventional, naive but intuitive explanation for the formation of Regge-trajectories does not apply in our framework. Nevertheless, we see an (approximate) ρ - and ϕ -meson Regge trajectory for our re-

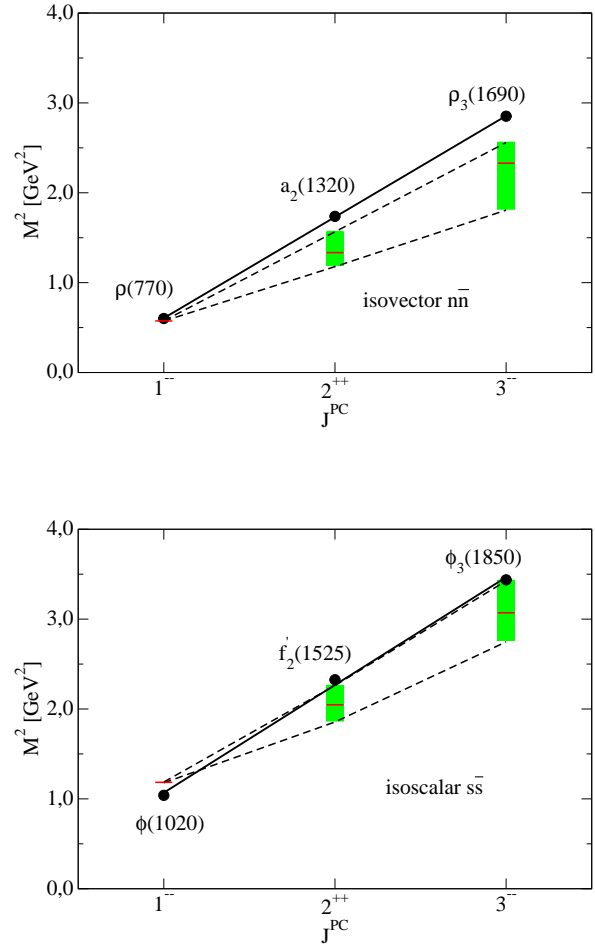


Fig. 8. Regge trajectories for isovector $n\bar{n}$ (upper plot) and isoscalar $s\bar{s}$ mesons (lower plot) with natural parity. Filled circles correspond to experimental data, while calculated values are given by the red marks for $\eta = 1.8$ and the green bands for $\eta = 1.8 \pm 0.2$. The resulting Regge trajectories for the upper and lower end of the bands are displayed by the dashed lines. Not shown is the numerical error of our mass extraction procedure, which is of the order of 5-10 % for the $J = 2, 3$ states.

sults. The slope of the trajectory is easily extracted. With

$$M_X^2(J) = M_X^2(0) + \beta_X J, \quad (31)$$

we find

$$\begin{aligned} M_\rho^2(0) &= -0.42 \text{ } (-0.05) \text{ GeV}^2, \\ \beta_\rho &= 0.99 \text{ } (0.62) \text{ GeV}^2, \end{aligned}$$

and

$$\begin{aligned} M_\phi^2(0) &= 0.05 \text{ } (0.36) \text{ GeV}^2, \\ \beta_\phi &= 1.12 \text{ } (0.78) \text{ GeV}^2, \end{aligned}$$

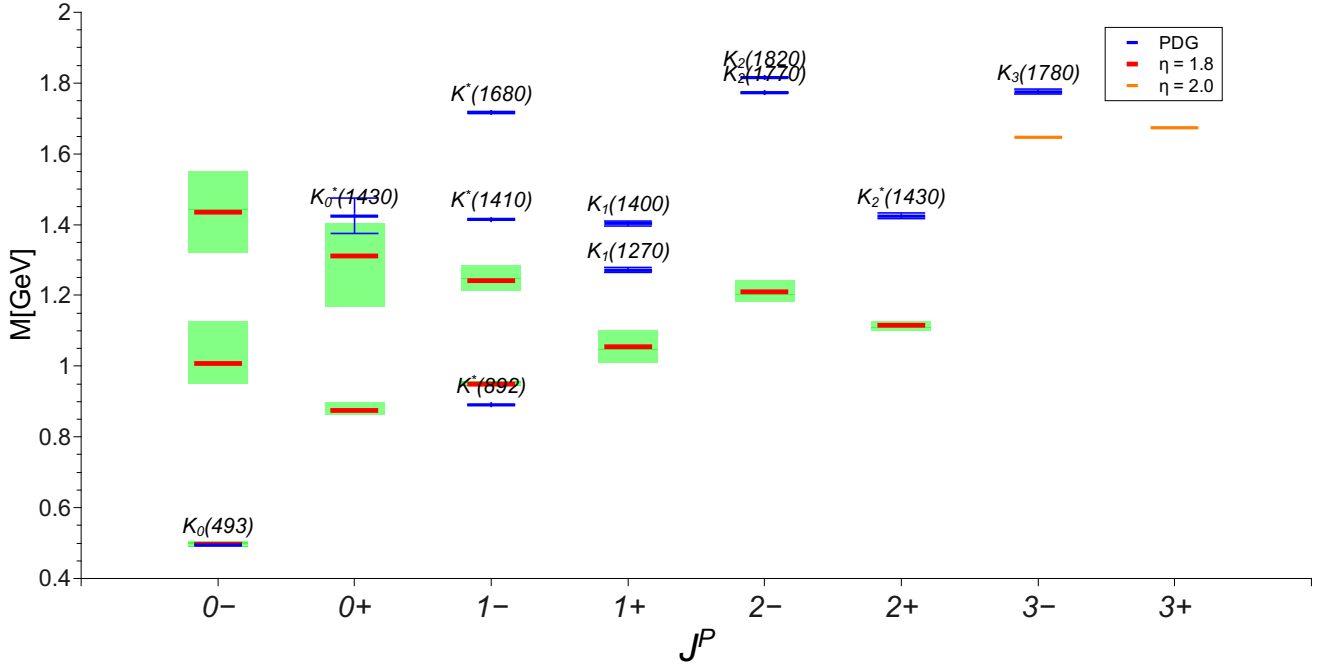


Fig. 7. (color online) Our calculated $n\bar{s}$ spectrum, compared to experiment. The green bands correspond to the variation $\eta = 1.8 \pm 0.2$. Due to the structure of the propagator, in the case of $\eta = 2.0$ more states are accessible; these are given by the single orange lines. The states to the right of the dividing line correspond to exotic quantum numbers.

for $X = \rho$ and $X = \phi$ respectively. The two numbers each correspond to the upper (lower) end of the η -band of our results. Compared to recent studies of Regge trajectories based on the ρ -meson, $\beta_\rho = 1.19 \pm 0.10 \text{ GeV}^2$ [37] and $\beta_\rho = 1.11 \pm 0.01 \text{ GeV}^2$ [38], our number for the slope at the upper edge of the η -band is smaller by only about ten percent. Recalling that we need to employ an extrapolation procedure in the complex momentum plane to extract the bound state mass of the tensor states with an error margin of the order of 5-10 % the agreement is quite good.

We have also checked for Regge trajectories in channels with unnatural parity and found an approximate linear trajectory also for the sequence $J^{PC} = 1^{++}, 2^{--}, 3^{++}$ based on the a_0 . Again, for the other channels and the excited states we find not enough bound states with $J = 2, 3$. From the discussion in the previous sections we furthermore expect, that the slopes and intercepts in these channels may be further off the experimentally extracted values, simply because the rainbow-ladder interaction is not good enough in these channels. Indeed for the a_0 -trajectory we find $M_{a_0}^2(0) = 0.20 \text{ GeV}^2$ and $\beta_{a_0} = 0.78 \text{ GeV}^2$ for the upper edge of the η -band, which do not agree too well with *e.g.* the values found in Ref. [7], $M_{a_0}^2(0) = -0.658 \pm 0.120 \text{ GeV}^2$ and $\beta_{a_0} = 1.014 \pm 0.036 \text{ GeV}^2$.

6 Summary and conclusions

We presented the covariant decomposition of $J \leq 3$ quark-antiquark bound states, following [2, 3] and [4]. Within the

rainbow-ladder truncations using a well-established effective interaction we calculated the spectrum of light unflavored and strange mesons. Comparison with experiment highlights the need to explore truncations beyond that of rainbow-ladder; in particular the effects of mixing as well as the introduction of a flavor dependent interaction are needed. In the language of potentials for the spin-spin and spin-orbit forces we find sizable deviations in all channels, where the tensor part of the spin-spin interaction is important. These are in particular the scalar and axialvector channels. On the other hand, the results are quantitatively reliable on the five percent level (at least for the upper end of the checked η -band of the interaction parameter) for channels where only the contact part of the spin-spin interaction plays a role, *i.e.* the hyperfine splitting of the S -states, and channels dominated by the spin-orbit force, *i.e.* $J^{PC} = 2^{++}, 3^{--}$. As a consequence, we find that the ground state Regge trajectory based on the ρ -meson agrees with extractions from experiment on the ten percent level. Since our approach is *not* based on a linear rising potential between light quarks, it is interesting that we see approximate Regge trajectories in the first place. This sheds some doubt on the intuitive but naive interpretation of Regge-behavior as originating from color flux tubes. The alternative mechanism at work in our framework needs to be explored further. Future work will also focus on the accessibility of excited states through a proper treatment of the quark propagator poles in both the quark DSE and meson BSE, in addition to

Table 2. Mass spectrum in MeV for isospin degenerate $n\bar{n}$, isoscalar $s\bar{s}$, and $I = 1/2$ $n\bar{s}$ bound-states. The rainbow ladder result corresponds to $\eta = 1.8 \pm 0.2$, with the superscript † (‡) indicating $\eta = 2.0$ ($\eta = 1.6$) only.

J^{PC}	$n\bar{n}$			$s\bar{s}$			J^P	$n\bar{s}$		
	$n = 0$	$n = 1$	$n = 2$	$n = 0$	$n = 1$	$n = 2$		$n = 0$	$n = 1$	$n = 2$
0^{-+}	$138.1^{+1.3}_{-0.6}$	1103.0^\dagger	1770.1^\dagger	$696.3^{+2.4}_{-1.7}$	$1426.3_{-76.6}$		0^-	$496.6^{+5.3}_{-0.9}$	$1007.6^{+118.3}_{-57.0}$	1435.9
0^{--}	$828.8^{+66.9}_{-57.1}$			$1133.8^{+68.0}_{-50.8}$						
0^{++}	$643.6^{+17.6}_{-37.6}$	1266.9^\dagger	1769.1^\dagger	$1079.4^{+1.7}_{-7.9}$	1643.6^\dagger		0^+	$874.5^{+10.0}_{-22.2}$	$1312.5^{+90.3}_{-143.8}$	
0^{+-}	$1035.5^{+66.8}_{-38.8}$			$1386.7^{+68.8}_{-37.9}$						
1^{-+}	$1043.9_{-37.0}$			$1347.3^{+73.2}_{-43.7}$	1870.1^\ddagger		1^-	$950.1^{+5.5}_{-1.6}$	$1241.6^{+43.5}_{-27.9}$	
1^{--}	$757.2^{+1.2}_{-0.6}$	$1022.6^{+9.2}_{-29.2}$	1331.9^\dagger	$1087.8^{+1.8}_{-2.2}$	$1413.1^{+38.8}_{-42.1}$	1666.9^\dagger				
1^{++}	$969.4^{+15.6}_{-23.9}$	1188.1^\dagger		$1301.0^{+34.7}_{-28.5}$	$1591.9^{+181.2}$		1^+	$1054.1^{+48.7}_{-44.8}$		
1^{+-}	$852.1^{+13.6}_{-5.2}$	$1017.4^{+0.6}_{-21.4}$	1345.2^\dagger	$1205.1^{+51.8}_{-46.6}$	$1372.0^{+34.4}_{-39.5}$	1831.6^\dagger				
2^{-+}	$1226.5^{+73.9}_{-80.0}$			$1513.5^{+90.5}_{-85.0}$			2^-	$1116.2^{+10.9}_{-17.2}$		
2^{--}	$1202.6^{+140.0}_{-94.3}$			$1484.7^{+76.0}_{-86.0}$						
2^{++}	$1154.8^{+96.5}_{-69.3}$			$1431.4^{+72.4}_{-69.3}$			2^+	$1209.4^{+32.3}_{-26.6}$		
2^{+-}										
3^{-+}				$1842.5_{-46.6}$			3^-	1646.9^\dagger		
3^{--}	$1528.3^{+71.2}_{-184.2}$			$1751.7^{+99.2}_{-94.3}$						
3^{++}	$1510.5^{+81.6}_{-100.3}$			$1770.9^{+91.4}_{-96.1}$			3^+	1673.4^\dagger		
3^{+-}				$1849.4_{-43.6}$						

an exploration of the heavy-heavy and heavy-light meson spectrum.

Acknowledgments

We thank Gernot Eichmann, Walter Heupel and Helios Sanchis-Alepuz for useful discussions. We are grateful to Christian Kellermann for valuable contributions in the early stage of the work. We thank Gernot Eichmann for comments and a critical reading of the manuscript. This work was supported by the Helmholtz International Center for FAIR within the LOEWE program of the State of Hesse, by the BMBF under contract No. 06GI7121, and the Austrian Science Fund (FWF) under project number M1333-N16.

A Supplementary Table

In Table 2 we collect together our results for $n\bar{n}$, $s\bar{s}$ and $n\bar{s}$ states.

References

1. N. Brambilla, S. Eidelman, P. Foka, S. Gardner, A. S. Kronfeld, M. G. Alford, R. Alkofer and M. Butenschön *et al.*, arXiv:1404.3723 [hep-ph].
2. H. Joos, Fortsch. Phys. **10** (1962) 65.
3. S. Weinberg, Phys. Rev. **133** (1964) B1318.
4. C. Zemach, Phys. Rev. **140** (1965) B97.
5. A. Krassnigg and M. Blank, Phys. Rev. D **83** (2011) 096006 [arXiv:1011.6650 [hep-ph]].
6. S. Godfrey and N. Isgur, Phys. Rev. D **32** (1985) 189.
7. D. Ebert, R. N. Faustov and V. O. Galkin, Phys. Rev. D **79** (2009) 114029 [arXiv:0903.5183 [hep-ph]].
8. S. -x. Qin, L. Chang, Y. -x. Liu, C. D. Roberts and D. J. Wilson, Phys. Rev. C **85** (2012) 035202 [arXiv:1109.3459 [nucl-th]].
9. M. Blank and A. Krassnigg, Phys. Rev. D **84** (2011) 096014 [arXiv:1109.6509 [hep-ph]].
10. A. Bender, C. D. Roberts and L. Von Smekal, Phys. Lett. B **380** (1996) 7 [nucl-th/9602012].
11. P. Watson, W. Cassing and P. C. Tandy, Few Body Syst. **35** (2004) 129 [hep-ph/0406340].
12. M. S. Bhagwat, A. Holl, A. Krassnigg, C. D. Roberts and P. C. Tandy, Phys. Rev. C **70** (2004) 035205 [nucl-th/0403012].
13. H. H. Matevosyan, A. W. Thomas and P. C. Tandy, Phys. Rev. C **75** (2007) 045201 [nucl-th/0605057].
14. R. Alkofer, C. S. Fischer, F. J. Llanes-Estrada and K. Schwenzer, Annals Phys. **324** (2009) 106 [arXiv:0804.3042 [hep-ph]].
15. C. S. Fischer, D. Nickel and J. Wambach, Phys. Rev. D **76** (2007) 094009 [arXiv:0705.4407 [hep-ph]].
16. C. S. Fischer and R. Williams, Phys. Rev. Lett. **103** (2009) 122001 [arXiv:0905.2291 [hep-ph]].
17. C. S. Fischer and R. Williams, Phys. Rev. D **78** (2008) 074006 [arXiv:0808.3372 [hep-ph]].
18. H. Sanchis-Alepuz, C. S. Fischer and S. Kubrak, Phys. Lett. B **733** (2014) 151 [arXiv:1401.3183 [hep-ph]].
19. L. Chang and C. D. Roberts, Phys. Rev. Lett. **103** (2009) 081601 [arXiv:0903.5461 [nucl-th]].

- 20. L. Chang, Y. -X. Liu and C. D. Roberts, Phys. Rev. Lett. **106** (2011) 072001 [arXiv:1009.3458 [nucl-th]].
- 21. L. Chang and C. D. Roberts, Phys. Rev. C **85** (2012) 052201 [arXiv:1104.4821 [nucl-th]].
- 22. W. Heupel, T. Goecke and C. S. Fischer, Eur. Phys. J. A **50** (2014) 85 [arXiv:1402.5042 [hep-ph]].
- 23. P. Maris and P. C. Tandy, Phys. Rev. C **60** (1999) 055214 [nucl-th/9905056].
- 24. C. H. Llewellyn-Smith, Annals Phys. **53** (1969) 521.
- 25. C. S. Fischer, P. Watson and W. Cassing, Phys. Rev. D **72** (2005) 094025 [hep-ph/0509213].
- 26. J-P. Berrut and L. N. Trefethen, SIAM Rev. **46** (2004) 501.
- 27. Gaël Guennebaud and Benoît Jacob *et al*, <http://eigen.tuxfamily.org> (2010)
- 28. L. Chang, I. C. Cloët, C. D. Roberts, S. M. Schmidt and P. C. Tandy, Phys. Rev. Lett. **111** (2013) 14, 141802 [arXiv:1307.0026 [nucl-th]].
- 29. S. M. Dorkin, L. P. Kaptari, T. Hilger and B. Kampf, Phys. Rev. C **89** (2014) 034005 [arXiv:1312.2721 [hep-ph]].
- 30. R. L. Jaffe, Phys. Rev. D **15** (1977) 267.
- 31. F. Giacosa, Phys. Rev. D **75** (2007) 054007 [hep-ph/0611388].
- 32. D. Ebert, R. N. Faustov and V. O. Galkin, Eur. Phys. J. C **60** (2009) 273 [arXiv:0812.2116 [hep-ph]].
- 33. D. Parganlija, P. Kovacs, G. Wolf, F. Giacosa and D. H. Rischke, Phys. Rev. D **87** (2013) 014011 [arXiv:1208.0585 [hep-ph]].
- 34. W. Heupel, G. Eichmann and C. S. Fischer, Phys. Lett. B **718** (2012) 545 [arXiv:1206.5129 [hep-ph]].
- 35. A. Holl, A. Krassnigg and C. D. Roberts, Phys. Rev. C **70** (2004) 042203 [nucl-th/0406030].
- 36. R. Alkofer, C. S. Fischer and R. Williams, Eur. Phys. J. A **38** (2008) 53 [arXiv:0804.3478 [hep-ph]].
- 37. P. Masjuan, E. Ruiz Arriola and W. Broniowski, Phys. Rev. D **85** (2012) 094006 [arXiv:1203.4782 [hep-ph]].
- 38. J. T. Londergan, J. Nebreda, J. R. Pelaez and A. Szczepaniak, Phys. Lett. B **729** (2014) 9 [arXiv:1311.7552 [hep-ph]].